



# Green Synthesis of Zinc Oxide and Copper Oxide Nanoparticles Using Aqueous Extract of Oak Fruit Hull (Jaft) and Comparing Their Photocatalytic Degradation of Basic Violet 3

Mina Sorbiun<sup>1</sup> · Ebrahim Shayegan Mehr<sup>1</sup> · Ali Ramazani<sup>1</sup> · Saeid Taghavi Fardood<sup>1</sup>

Received: 5 October 2017 / Revised: 25 November 2017 / Accepted: 2 January 2018  
© University of Tehran 2018

## Abstract

Here we report green synthesis of highly crystalline ZnO and CuO nanoparticles (NPs) by oak fruit hull (Jaft) as reducing and stabilizing agent. This method is nontoxic, eco-friendly and low cost in comparison with chemical and/or physical techniques. The characterization of obtained particles was studied by using field emission scanning electron microscopy (FESEM), X-ray diffraction analysis and Fourier transform infrared spectroscopy. The results indicating that NPs synthesized by Jaft extract have high purity and the average particle size is 34 nm. The ZnO NPs exhibited photocatalytic activity higher than CuO NPs for degradation of basic violet 3 dye in water at room temperature. The amount of basic violet 3 dye degradation by metal oxide NPs were studied by employing UV–Vis spectroscopy. Furthermore, the degradation of basic violet 3 using metal oxide NPs followed pseudo-first-order kinetics.

**Keywords** Zinc oxide nanoparticles · Copper oxide nanoparticles · Jaft · Basic violet 3 · Photocatalytic degradation

## Introduction

Metal nanoparticles usually display uncommon physical, chemical and biological properties compared to their macroscopic equivalents. The unique properties arise from particularly their high surface to volume ratio (Khan et al. 2016; Masoudpanah and Mirkazemi 2017). Nanotechnology is one of the most versatile areas of current research and has wide-ranging applications. A number of toxic physio-chemical techniques, such as spray pyrolysis, gas phase methods, chemical vapor deposition, electrochemical methods, and laser ablation techniques have been introduced to synthesize nanoparticles (Ahmadi Golsefidi et al. 2016; Asghari and Mohammadnia 2016; Borhade et al. 2014; Enhessari et al. 2011; Yuan et al. 2008). However, those methods always involve utilization of hazardous organic solvents, toxic reagents, non-biodegradable stabilizing agents and expensive instruments along with the

tedious process control. Therefore, there is a great attention to produce NPs using simple and safe green methods. Among the biological methods, plant-mediated synthesis of NPs are more attractive because of its simplicity, easy availability and stability of the resulting products. Plants are better suited for the synthesis of metal oxide nanoparticles than any other sources due to the presence of abundant secondary metabolites and easy reduction of their salts (Balraj et al. 2017; Elemike et al. 2017; Khaghani et al. 2017; Taghavi Fardood et al. 2017b, c, d).

Environmental pollution and particularly water pollution on a global scale have drawn scientists' attention to the vital need for environmentally clean and friendly chemical processes. Photocatalysts has been used extensively to decompose organic dyes, which is one of the main groups of pollutants in wastewaters to convert them into less hazardous or even nontoxic chemicals have been demonstrated to minimize the damage caused by organic dye contamination to the environment and humans (Ali et al. 2013; Luan et al. 2006; Sivakumar et al. 2014; Taghavi Fardood et al. 2017a). In recent years, attentions has been concentrated on the use of semiconductor materials as photocatalysts for the elimination of organic and inorganic

✉ Ali Ramazani  
aliramazani@gmail.com

<sup>1</sup> Department of Chemistry, University of Zanjan,  
P O Box 45195-313, Zanjan, Iran

species from aqueous or gas phase (Assi et al. 2017; Karimi and Zohoori 2013; Musa et al. 2012).

In this study, we synthesized zinc oxide and copper oxide nanoparticles (ZnO and CuO NPs) using extract of oak fruit hull (Jaft). The present method is rapid, environmentally benign and cost-effective when compared to chemical/physical method of ZnO, CuO NPs synthesis. All the characterization studies clearly proved the formation of nanoparticles. In addition, the photocatalytic activity of ZnO and CuO nanoparticles towards the degradation of basic violet 3 in aqueous solution under visible radiation was studied. The results showed that catalytic activity of ZnO being more effective than CuO for degradation of basic violet 3. The chemical structure and characteristics of basic violet 3 dye are listed in Table 1.

## Experimental

### Materials

Fruits of oak trees were collected from Zagros Mountains in the southwest of Iran and high pure analytical grade chemicals, such as copper (II) acetate monohydrate ( $\text{Cu}(\text{CH}_3\text{COO})_2 \cdot \text{H}_2\text{O}$ ) and zinc acetate dihydrate ( $\text{Zn}(\text{CH}_3\text{COO})_2 \cdot 2\text{H}_2\text{O}$ ) were purchased from daijung (Darmstadt, Korea). X-ray powder diffraction (XRD) technique on X'Pert-PRO advanced diffractometer using  $\text{Cu-K}\alpha$  radiation ( $\lambda = 1.5406 \text{ \AA}$ ) was used for phase identification of ZnO and CuO NP crystals and to obtain information on unit cell dimensions. Surface structure of all samples was characterized by a Jasco 6300 Fourier

transform infrared (FT-IR) spectroscope. Measurements were performed with pressed pellets made using KBr powder as diluent. The FT-IR spectrum was collected between the wave number of 400 and  $4000 \text{ cm}^{-1}$ . The surface morphology of as synthesized products was characterized by field emission scanning electron microscopy analysis (BRUKER- XFlash 6130). UV-Vis absorption spectra were prepared on a Metrohm (Analytical Jena-Specord 205) double beam instrument with a range of 400–700 nm operated at a resolution of 2 nm was utilized to monitor the degradation of dye.

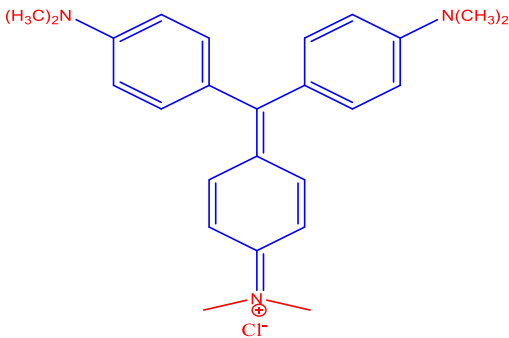
### Preparation of Aqueous Extract

Fruits of oak trees were washed with running tap water to remove dirt and shade dried. For the preparation of extract, 20 g of oak fruit hull (Jaft) (Fig. 1) was added in 100 mL of distilled water and boiled for 5 min. after boiling, the color of the aqueous solution was dark brown and the mixture was allowed to cool to room temperature. Then, the aqueous extract of Jaft was filtered by (Whatman No. 1) filter paper. The extract was stored at  $4^\circ\text{C}$  for further use.

### Synthesis of CuO Nanoparticles

To synthesize CuO NPs, in brief, 30 mL of Jaft extract was heated to  $70^\circ\text{C}$  using water bath under stirring. Then 1 g of copper (II) acetate monohydrate ( $\text{Cu}(\text{CH}_3\text{COO})_2 \cdot \text{H}_2\text{O}$ ) was dissolved in the extract under constant stirring. This solution was boiled until a brown-colored glue was formed. The glue was gathered in a ceramic vessel and heated in an air-heated furnace at  $500^\circ\text{C}$  for 4 h to obtain the CuO NPs.

**Table 1** Structure and characteristics of basic violet 3

Molecular structure	Triarylmethane class
Molecular formula	$\text{C}_{25}\text{H}_{30}\text{ClN}_3$
Molecular weight	407.98 g/mol
CAS registry number	548-62-9
$\lambda_{\text{max}}$	590 nm
Structure	

The black-colored powder samples were used for further studies.

### Synthesis of ZnO Nanoparticles

Briefly, 30 mL of Jaft extract was taken from the stock solution and heated at 60–80 °C using water bath. When the temperature of the solution reached 60 °C, 1 g of zinc acetate dihydrate ( $\text{Zn}(\text{CH}_3\text{COO})_2 \cdot 2\text{H}_2\text{O}$ ) was added into the hot Jaft extract with constant stirring for 4 h and light brown-colored solution was formed immediately. After 4 h, the culture solution was taken from the heat and allowed to cool at room temperature overnight. Next day, the reaction mixture was centrifuged at 4000 rpm for 20 min. The supernatant phase was removed and NPs were washed with 10 mL of water for three times to remove unwanted substances from the NPs. After the washing, the precipitate was dried in a hot-air oven at 80 °C for 6 h to obtain the product in the powder form. The obtained powders were calcinated at 500 °C for 4 h, and finally white powders were resulted.

### Photocatalytic Reactor

Experiments were carried out in a batch mode photoreactor. The irradiation source was a fluorescent lamp ( $\lambda > 400$  nm, 80 W, Pars, Iran), which was put above the batch photoreactor. The reaction was made in conditions: Basic violet 3 = 100 mg/L, catalyst = 0.05 g, pH = natural and room temperature.

### Photocatalytic Dye Degradation

The comparison of photocatalytic activity of the biologically synthesized ZnO/CuO was evaluated by measuring the photocatalytic degradation of basic violet 3 dye in water under the illumination of visible light. The photoreactions were conducted in a Pyrex flask type reactor under fluorescent lamp at room temperature and natural pH. For the effective degradation of basic violet 3 dye, 50 mg of the synthesized CuO and ZnO NPs was added in 50 mL of 100 ppm solution of basic violet 3 under constant stirring. Prior to visible illumination, the suspension was continuously stirred for about 0.5 h to develop adsorption–desorption equilibrium between basic violet 3 dye and photocatalyst under dark condition. Then, the stable aqueous dye solution was exposed to light illumination under constant stirring. The samples were withdrawn from the reaction medium at regular time interval. Before analysis, the aqueous samples were centrifuged at 4000 rpm for 12 min to settle down the catalyst particles at the bottom of the test tube before analysis. Finally, the absorption spectrum of decomposed dye was collected using a UV–visible

spectrophotometer (Analytical Jena-Specord 205). The photocatalytic degradation percentage of basic violet 3 was calculated by the following equation:

$$\text{photodegradation \%} = (C_0 - C/C_0)100 \quad (1)$$

where  $C_0$  and  $C$  are the UV–Vis absorption of original and sampled solutions, respectively. Moreover, photocatalytic degradation of basic violet 3 dye followed the pseudo-first-order kinetics and rate constant was determined by the following relation:

$$\ln(C_0/C_t) = kt \quad (2)$$

the  $k$  was calculated from the graph between  $\ln(C_0/C_t)$  vs time interval, where  $C_0$  is the initial absorbance of dye solution, and  $C_t$  is the absorbance of dye solution after irradiation at time  $t$ .

To check whether the basic violet 3 is easily degradable or not, blank experiment (without addition of any catalyst) has also been done. Results showed insignificant changes were observed for the duration of 120 min (< 10%). This showed that the dye in the solution was very stable and do not have self-destruct mechanism even if it was irradiated under the light sources for 2 h (Teka and Reda 2014).

## Results and Discussion

### FESEM

The surface morphology of as synthesized CuO and ZnO samples was primarily characterized by field emission scanning electron microscopic (FESEM) analysis. The biosynthesized CuO and ZnO NPs were observed using FESEM and the resultant images are shown in Fig. 2. It can be observed that most of the CuO nanoparticles are in nanometer scale and are mostly of quasi-spherical shape (Fig. 2a, b). The synthesized ZnO nanostructures possess highly uniform spherical particles with the average

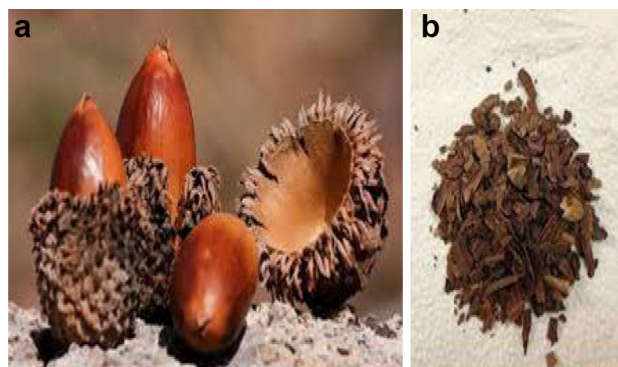
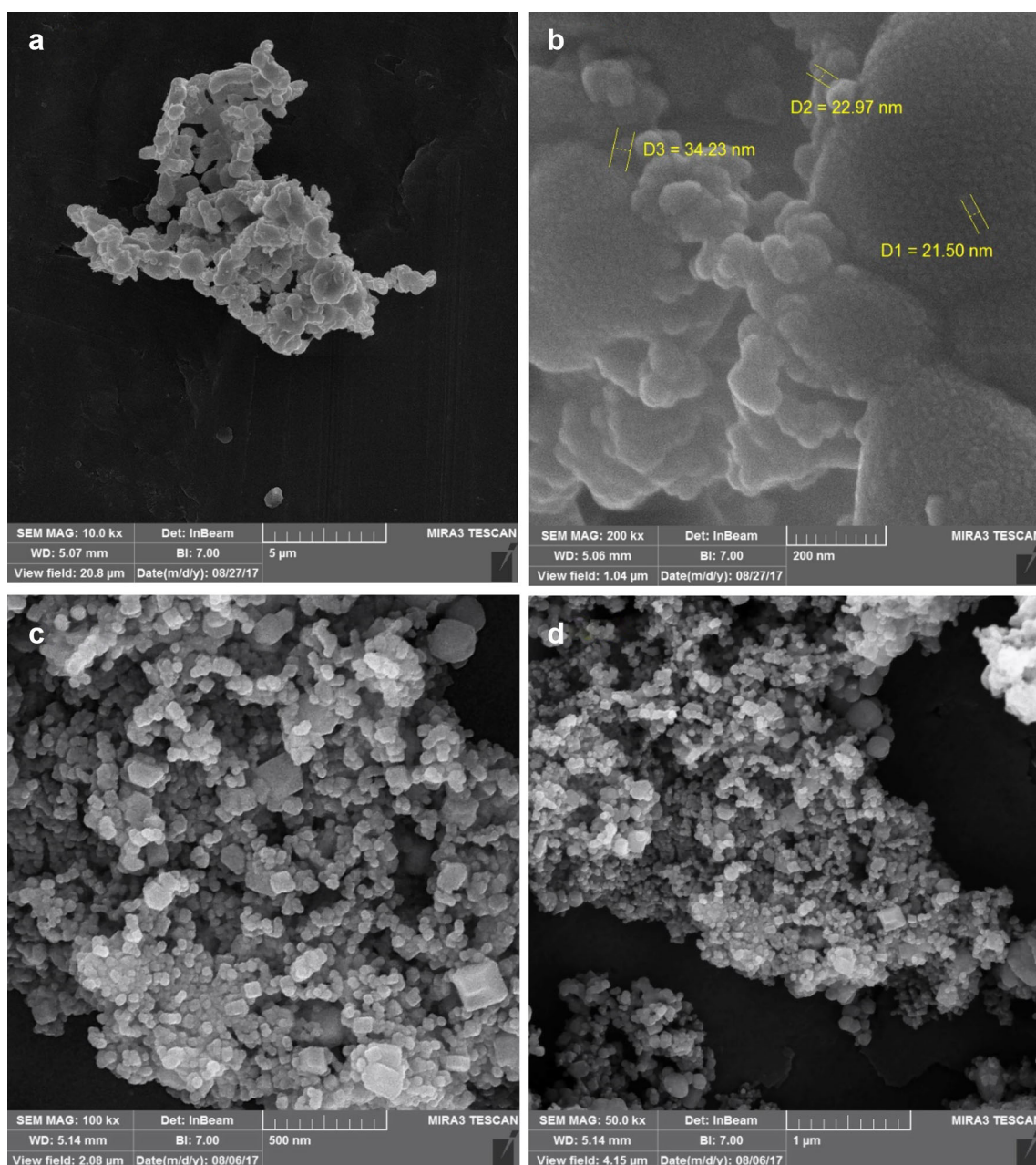


Fig. 1 Images of oak fruit (a) and Jaft (b)



**Fig. 2** FESEM images of CuO NPs (**a**, **b**) and ZnO NPs (**c**, **d**) calcined at 500 °C

diameter of 34 nm. Noticeably, most of the nanoparticles are uniform in size along with a few big particles (Fig. 2c, d). The NPs are little agglomerated and the size of the CuO and ZnO NPs has increased slightly after annealing.

### X-ray Diffraction

Figure 3a shows the X-ray diffraction patterns of ZnO NPs. The  $2\theta$  characteristic peaks of ZnO at  $31.28^\circ$ ,  $33.88^\circ$ ,  $35.71^\circ$ ,  $46.98^\circ$ ,  $56.08^\circ$ ,  $62.36^\circ$ ,  $65.89^\circ$ ,  $67.44^\circ$ ,  $68.69^\circ$ ,  $72.02^\circ$  and  $76.38^\circ$  corresponding to the (100), (002), (101),

(102), (110), (103), (200), (112), (201), (004) and (202) planes of the crystal lattice, respectively. The results of the XRD analysis are in accordance with JCPDS No: 00-036-1451 suggesting the typical hexagonal wurtzite phase with the lattice parameters  $a = b = 3.2498$  and  $c = 5.2066$  Å. The average crystallite size of ZnO NPs was also estimated by the Debye–Scherrer equation  $D = K\lambda/\beta \cos \theta$ , where,  $K$  is a constant (0.94),  $\lambda$  is the wavelength (Cu  $K\alpha = 0.154171$  nm),  $\theta$  is the Bragg angle and  $\beta$  the full width at half maxima (FWHM) of a diffracted peak. By taking the FWHM at (101), the average crystallite size is



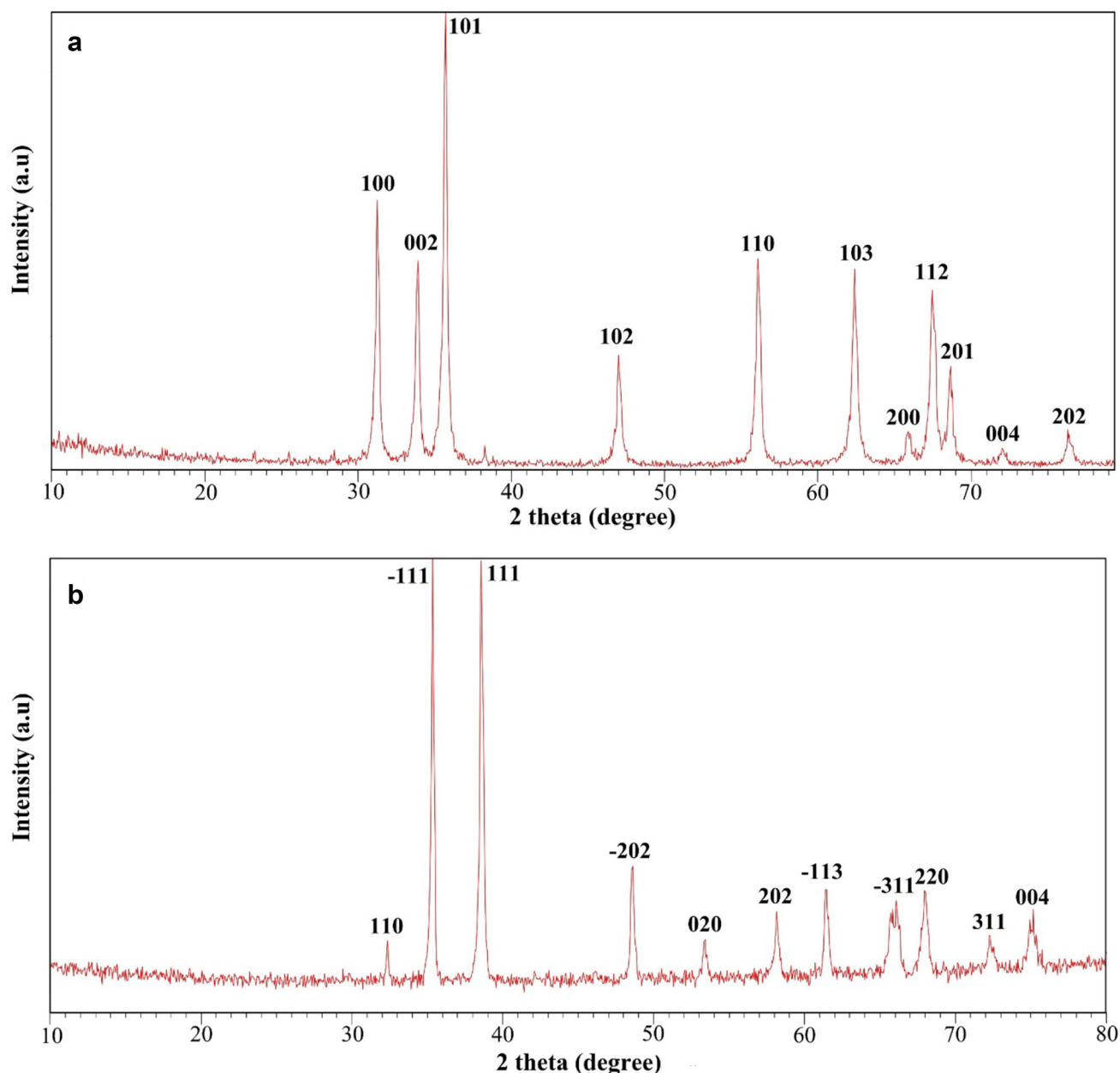


**Fig. 3** XRD patterns of **a** ZnO NPs and **b** CuO NPs calcined at 500 °C

found to be 44 nm, which is consistent with FESEM results. Figure 3b represents the XRD pattern of biosynthesized CuO NPs, the peaks at 32.34°, 35.36°, 38.56°, 48.57°, 53.39°, 58.14°, 61.40°, 66.17°, 67.98°, 72.48°, and 75.02° were assigned to planes of (110), (− 111), (111), (− 202), (020), (202), (− 113), (− 311), (220), (311) and (004), respectively. All the peaks are confirmed CuO monoclinic phase by comparison with JCPDS card No. 01-080-1268. The sharp and narrow diffraction peaks indicate the product is well crystalline in nature. The synthesized CuO NPs were found to be pure, without any impurities. The average crystallite size (*D*) of CuO NPs

was calculated to be about 40 nm using Scherer formula. Where  $\lambda$  is the wavelength (Cu K $\alpha$ ),  $\lambda$  is the full width half maximum (FWHM) of CuO (− 111) line and  $\theta$  is diffraction angle.

### FTIR Spectra

FTIR analysis was carried out to identify the possible biomolecules involved in the biosynthesis of ZnO and CuO NPs. The FTIR spectra of the analyzed samples are displayed in Figs. 4 and 5. The spectrum obtained for synthesis ZnO NPs (Fig. 4) clearly shows ZnO absorption

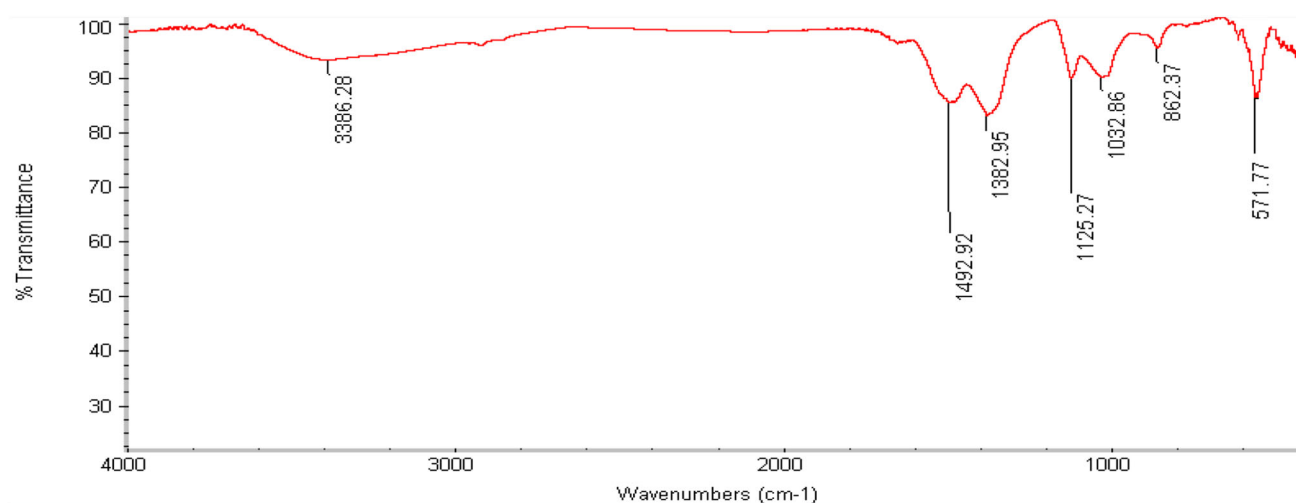


Fig. 4 FTIR spectrum of ZnO NPs

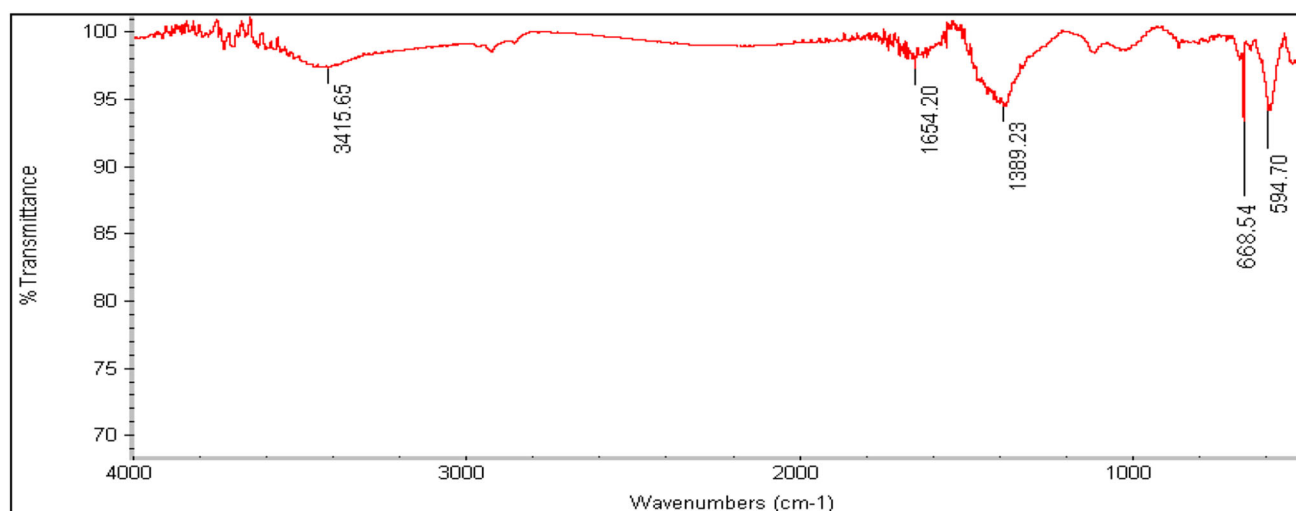


Fig. 5 FTIR spectrum of CuO NPs

band near  $571\text{ cm}^{-1}$  (Taghavi Fardood et al. 2017e). The peaks were observed at 1032, 1125 and  $1382\text{ cm}^{-1}$  can be ascribed to alcohols, phenolic groups and C–N stretching vibrations of aliphatic and aromatic amines, respectively. The peak around  $1492\text{ cm}^{-1}$  is due to the amide I bonds of proteins or enzymes (Tingfa 1989). The band at  $3386\text{ cm}^{-1}$  is representing to O–H stretching alcohol or phenol group. The absorption peak around  $860\text{ cm}^{-1}$  probably due to O–H functional group (Yildiz et al. 2014).

The FT-IR spectral peak of CuO NPs was recorded in the range of  $4000\text{--}400\text{ cm}^{-1}$  using KBr disc method (Fig. 5). The broad band around  $3415\text{ cm}^{-1}$  corresponds to the O–H stretching polyphenols (flavonoids) present in the plant extract (Raghuveeran et al. 2011). Peak at  $1654\text{ cm}^{-1}$  corresponds to amide I stretching vibrations. Peak at  $1389\text{ cm}^{-1}$  represent the O–C–O stretching modes

of vibration of esters (Das and Velusamy 2013). The bands at  $800\text{--}600\text{ cm}^{-1}$  region (for C–H out of plane bend) which are of characteristic of aromatic phenols. This can be attributed to the adsorption of phenolic compound such as tannic acid product on the CuO NPs surface which may be responsible for the capping and particle stabilization (Chang Chien et al. 2007). The peaks in region between 500 and  $600\text{ cm}^{-1}$  are allotted to metal–oxygen vibration (Taghavi Fardood and Ramazani 2016).

### Photocatalytic Degradation of Basic Violet 3 in the Presence of the ZnO and CuO NPs

The photodegradation of dye under simulated visible light was studied by measuring the decrease in the absorbance of the dye in presence of the prepared nanopowders. The

**Fig. 6** Absorption spectra of 100 ppm solutions of basic violet 3 in the presence of 0.05 g of **a** CuO and **b** ZnO photocatalyst under visible light radiation

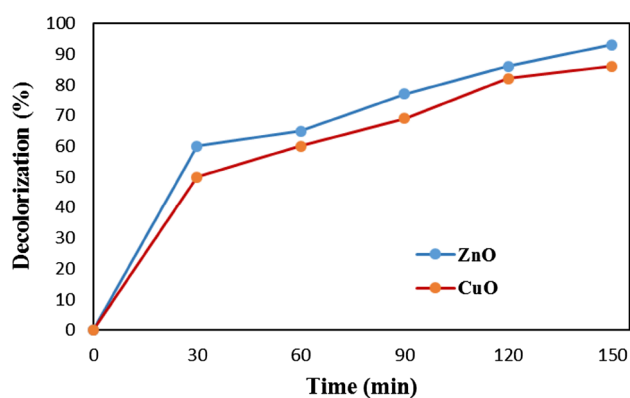
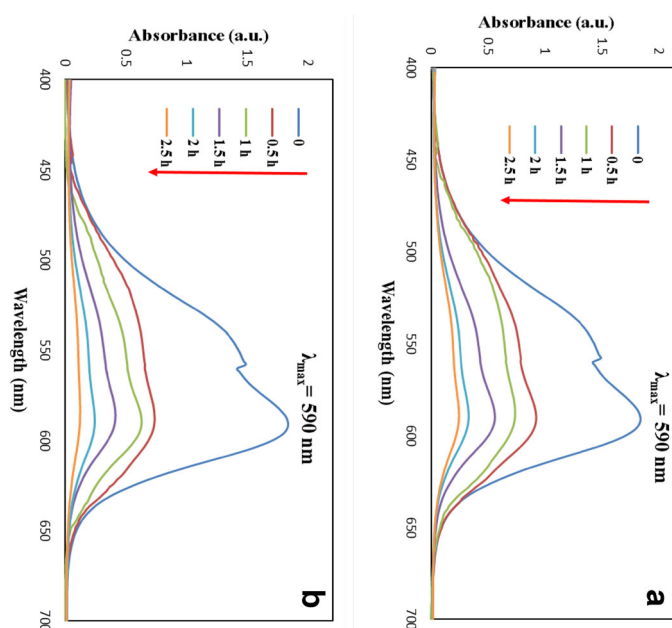


**Fig. 7** Percentage decolorization of basic violet 3 in the presence of ZnO and CuO NPs

**Table 2** Degradation efficiency of ZnO and CuO for removal of basic violet 3 under the visible light irradiation

Time (h)	0.5	1	1.30	2	2.30
photodegradation % by CuO NPs	50	60	69	82	86
photodegradation % by ZnO NPs	60	65	77	86	93

absorbance of the dye solution decreased with increasing time of exposure, indicating a decrease in the concentration of basic violet 3 dye (Fig. 6). The time-dependent degradation of basic violet 3 for the samples under visible light irradiation are shown in Fig. 7. The dye degradation (%) was calculated using the Eq. 1 (Table 2).

The plots of  $\ln(C_0/C)$  versus irradiation time ( $t$ ) was linear. Figure 8 shows that the photocatalytic degradation

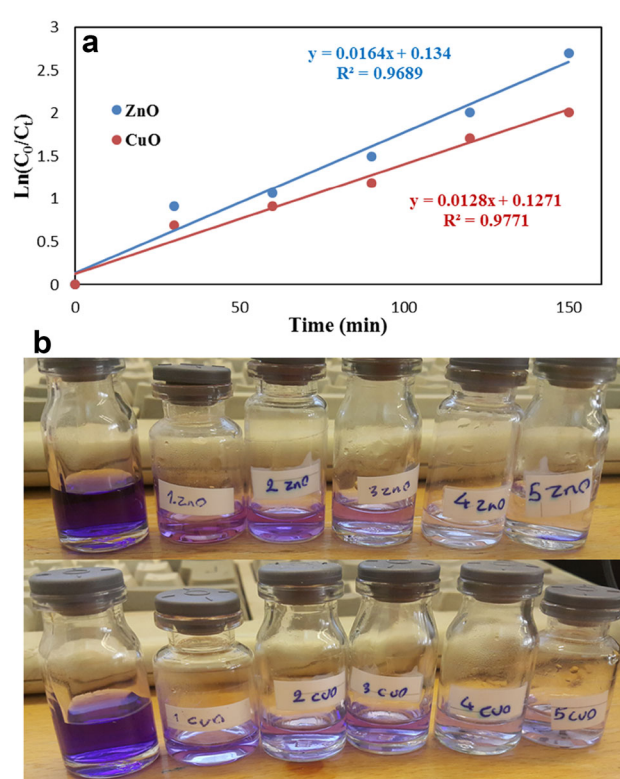


**Fig. 8** **a** Kinetics of photodegradation of the basic violet 3 dye. **b** The gradual decolourization of the basic violet 3 dye by the ZnO and CuO catalyst. (Reaction conditions: Basic violet 3 = 100 mg/L, catalyst = 0.05 g, pH = natural and room temperature.)

of basic violet 3 approximately follows first-order reaction kinetics. This corresponded to a rate constant of 0.0164 and 0.0128  $\text{min}^{-1}$  for ZnO and CuO, respectively.

## Conclusion

In conclusion, we show an environmentally friendly method to prepare stable ZnO, CuO nanoparticles employing Jaft extract without usage of any special capping agents. The synthesized ZnO, CuO nanoparticles capped by biomolecules was characterized by FESEM, XRD and FT-IR. The spherical-like and quasi-cubic morphology of ZnO and CuO NPs was confirmed by FESEM, respectively. The presence of hexagonal wurtzite phase of ZnO NPs and monoclinic phase of CuO NPs was confirmed by XRD. The observed vibration peaks in the FT-IR analysis indicated the presence of metal–oxygen species. The advantages of this biosynthesis method include (1) use of plant extract as an economic and effective alternative, (2) use of cheap, clean, nontoxic and environmentally benign precursors and (3) simple procedures without application of toxic reagents or surfactant template. In addition, the catalytic activity of ZnO and CuO NPs for degradation of basic violet 3 was also studied. A comparative photocatalytic activity study has been conducted for the ZnO and CuO nanomaterial samples. The results showed that ZnO exhibited the higher photocatalytic activity than CuO. Of course, the degradation rate values were high for both samples. This study offers a low-cost, eco-friendly solution to water purification problem.

## References

- Ahmadi Golsefidi M, Yazarlou F, Naeimi Nezamabad M, Naeimi Nezamabad B, Karimi M (2016) Effects of capping agent and surfactant on the morphology and size of  $\text{CoFe}_2\text{O}_4$  nanostructures and photocatalyst properties. *J Nanostruct* 6:121–126. <https://doi.org/10.7508/jns.2016.02.003>
- Ali MA, Idris MR, Quayum ME (2013) Fabrication of ZnO nanoparticles by solution-combustion method for the photocatalytic degradation of organic dye. *J Nanostruct Chem* 3:36. <https://doi.org/10.1186/2193-8865-3-36>
- Asghari S, Mohammadnia M (2016) Synthesis and characterization of pyridine-4-carboxylic acid functionalized  $\text{Fe}_3\text{O}_4$  nanoparticles as a magnetic catalyst for synthesis of pyrano[3,2-b]pyranone derivatives under solvent-free conditions. *Res Chem Intermed* 42:1899–1911. <https://doi.org/10.1007/s11164-015-2124-0>
- Assi H, Atiq S, Rammay SM, Alzayed NS, Saleem M, Riaz S, Naseem S (2017) Substituted Mg–Co-nanoferrite: recyclable magnetic photocatalyst for the reduction of methylene blue and degradation of toxic dyes. *J Mater Sci Mater Electron* 28:2250–2256. <https://doi.org/10.1007/s10854-016-5795-4>
- Balraj B, Senthilkumar N, Siva C, Krithikadevi R, Julie A, Potheher IV, Arulmozhi M (2017) Synthesis and characterization of zinc oxide nanoparticles using marine *Streptomyces* sp. with its investigations on anticancer and antibacterial activity. *Res Chem Intermed* 43:2367–2376. <https://doi.org/10.1007/s11164-016-2766-6>
- Borhade AV, Uphade BK, Tope DR (2014) Synthesis, characterization, and catalytic application of PbS nanoparticles for the synthesis of amidoalkyl naphthols under solvent-free conditions. *Res Chem Intermed* 40:211–223. <https://doi.org/10.1007/s11164-012-0956-4>
- Chang Chien S, Wang M, Huang C, Seshiah K (2007) Characterization of humic substances derived from swine manure-based compost and correlation of their characteristics with reactivities with heavy metals. *J Agric Food Chem* 55:4820–4827. <https://doi.org/10.1021/jf070021d>
- Das J, Velusamy P (2013) Antibacterial effects of biosynthesized silver nanoparticles using aqueous leaf extract of *Rosmarinus officinalis* L. *Mater Res Bull* 48:4531–4537. <https://doi.org/10.1016/j.materresbull.2013.07.049>
- Elemike EE, Onwudiwe DC, Ekenia AC, Katata-Seru L (2017) Biosynthesis, characterization, and antimicrobial effect of silver nanoparticles obtained using *Lavandula* × *intermedia*. *Res Chem Intermed* 43:1383–1394. <https://doi.org/10.1007/s11164-016-2704-7>
- Enhessari M, Kargar-Razi M, Moarefi P, Parviz A (2011) Synthesis, characterization and photocatalytic properties of  $\text{MnTiO}_3$ -zeolite-Y nanocomposites. *J Nanostruct* 1:119–125. <https://doi.org/10.7508/jns.2011.02.005>
- Karimi L, Zohoori S (2013) Superior photocatalytic degradation of azo dyes in aqueous solutions using  $\text{TiO}_2/\text{SrTiO}_3$  nanocomposite. *J Nanostruct Chem* 3:32. <https://doi.org/10.1186/2193-8865-3-32>
- Khaghani S, Ghanbari D, Khaghani S (2017) Green synthesis of iron oxide-palladium nanocomposites by pepper extract and its application in removing of colored pollutants from water. *J Nanostruct* 7:175–182
- Khan ST, Musarrat J, Al-Khedhairy AA (2016) Countering drug resistance, infectious diseases, and sepsis using metal and metal oxides nanoparticles: current status. *Colloids Surf B* 146:70–83. <https://doi.org/10.1016/j.colsurfb.2016.05.046>
- Luan J, Zou Z, Lu M, Luan G, Chen Y (2006) Structural and photocatalytic properties of the new solid photocatalyst  $\text{In}_2\text{BiTaO}_7$ . *Res Chem Intermed* 32:31–42. <https://doi.org/10.1163/156856706775012950>
- Masoudpanah SM, Mirkazemi SM (2017) Structural, magnetic and photocatalytic properties of  $\text{BiFeO}_3$  nanoparticles. *J Nanostruct* 7:183–188
- Musa AY, Ba-Abbad MM, Kadhum AAH, Mohamad AB (2012) Photodegradation of chlorophenolic compounds using zinc oxide as photocatalyst: experimental and theoretical studies. *Res Chem Intermed* 38:995–1005. <https://doi.org/10.1007/s11164-011-0435-3>
- Raghunandan D, Mahesh BD, Basavaraja S, Balaji S, Manjunath S, Venkataraman A (2011) Microwave-assisted rapid extracellular synthesis of stable bio-functionalized silver nanoparticles from guava (*Psidium guajava*) leaf extract. *J Nanopart Res* 13:2021–2028. <https://doi.org/10.1007/s11051-010-9956-8>
- Sivakumar P, Gaurav Kumar GK, Sivakumar P, Renganathan S (2014) Synthesis and characterization of ZnS–Ag nanoballs and its application in photocatalytic dye degradation under visible light. *J Nanostruct Chem* 4:107. <https://doi.org/10.1007/s40097-014-0107-0>
- Taghavi Fardood S, Ramazani A (2016) Green synthesis and characterization of copper oxide nanoparticles using coffee powder. *Extract J Nanostruct* 6:167–171
- Taghavi Fardood S, Atrak K, Ramazani A (2017a) Green synthesis using tragacanth gum and characterization of Ni–Cu–Zn ferrite nanoparticles as a magnetically separable photocatalyst for organic dyes degradation from aqueous solution under visible light. *J Mater Sci Mater Electron* 28:10739–10746. <https://doi.org/10.1007/s10854-017-6850-5>



- Taghavi Fardood S, Ramazani A, Golfar Z, Joo SW (2017b) Green synthesis of  $\alpha$ -Fe<sub>2</sub>O<sub>3</sub> (hematite) nanoparticles using tragacanth. *Gel J Appl Chem Res* 11:19–27
- Taghavi Fardood S, Ramazani A, Moradi S (2017c) Green synthesis of Ni–Cu–Mg ferrite nanoparticles using tragacanth gum and their use as an efficient catalyst for the synthesis of polyhydroquinoline derivatives. *J Sol-Gel Sci Technol* 82:432–439. <https://doi.org/10.1007/s10971-017-4310-6>
- Taghavi Fardood S, Ramazani A, Moradi S (2017d) A novel green synthesis of nickel oxide nanoparticles using Arabic Gum. *Chem J Mold* 12:115–118. <https://doi.org/10.19261/cjm.2017.383>
- Taghavi Fardood S, Ramazani A, Moradi S, Azimzadeh Asiabi P (2017e) Green synthesis of zinc oxide nanoparticles using arabic gum and photocatalytic degradation of direct blue 129 dye under visible light. *J Mater Sci Mater Electron* 28:13596–13601. <https://doi.org/10.1007/s10854-017-7199-5>
- Teka T, Reda A (2014) Comparative study on the photocatalytic degradation of malachite green using zinc oxide under different sources of radiation. *IJTEEE* 2:6–9
- Tingfa D (1989) Thermal decomposition studies of solid propellant binder HTPB. *Thermochim Acta* 138:189–197. [https://doi.org/10.1016/0040-6031\(89\)87255-7](https://doi.org/10.1016/0040-6031(89)87255-7)
- Yıldız N, Ateş Ç, Yılmaz M, Demir D, Yıldız A, Çalıklı A (2014) Investigation of lichen based green synthesis of silver nanoparticles with response surface methodology. *Green Process Synth* 3:259–270. <https://doi.org/10.1515/gps-2014-0024>
- Yuan S, Kawasaki S, Mori K, Yamashita H (2008) Synthesis and photocatalytic activity of TiO<sub>2</sub> nanoparticles fluorine-modified with TiF<sub>4</sub>. *Res Chem Intermed* 34:331–337. <https://doi.org/10.1163/156856708784040687>